Acta Crystallographica Section B
Structural Science
ISSN 0108-7681

Calcium–lead fluoro-vanadinite apatites. II. Equilibrium structures

ZhiLi Dong* and T. J. White

Centre for Advanced Research of Ecomaterials, Institute of Environmental Science and Engineering, Innovation Centre, Nanyang Technological University, Block 2, Unit 237, 18 Nanyang Drive, Singapore 637723, Singapore

Correspondence e-mail: zldong@ntu.edu.sg

Received 27 November 2003
Accepted 24 January 2004

The synthetic vanadinites $(Pb_xCa_{10-x})(VO_4)_6(F_{1-2y}O_y\square_y)_2$, $0.57 < x < 9$ and $0.10 < y < 0.47$, adopt the $P6_3/m$ apatite structure with $9.7835\,(3) \leq a \leq 10.0531\,(1)$ Å and $7.0318\,(2) \leq c \leq 7.3033\,(1)$ Å. The calcium endmember is monoclinic, space group $P2_1/m$, with $a = 9.7370\,(3)$, $b = 9.7358\,(4)$, $c = 7.00572\,(9)$ Å, $\gamma = 120.002\,(5)^\circ$. For mixed metal compounds ($x \neq 0$) the partitioning of calcium and lead over the $A^{\rm I}(4f)$ and $A^{\rm II}(6h)$ positions is nonstoichiometric, with lead preferentially favouring the larger $A^{\rm II}$ site at a partitioning coefficient $k_{\rm Pb}(A^{\rm I}/A^{\rm II}) \simeq 0.33$ for all $x < 7$. A miscibility gap exists for $2 < x < 3$. Trends in crystallographic parameters can be correlated through consideration of the $A^{\rm I}O_6$ metaprism twist angle (φ) that can be used to derive ideal cell parameters from triangular anion networks.

1. Introduction

An established principle of toxic and radioactive waste management by synthetic mineral immobilization is that crystallochemical modifications at the unit-cell scale considerably enhance the capacity of ceramics to respond flexibly to variations in waste stream composition (White *et al.*, 1985). Developing a sound understanding of the mechanisms that permit departures from conventional solid solutions is an essential facet of validating and predicting the performance of crystalline waste forms and recycled materials. This is especially so for secondary products derived from industrial processes, such as incineration, since stabilization is usually accomplished under conditions that depart significantly from a thermodynamic and kinetic equilibrium. The impacts of disequilibrium on product performance are rarely addressed. This study was undertaken as part of a larger investigation to determine baseline structure constants of equilibrated waste-form apatites, whose diverse chemistry make them candidates for the treatment of a wide range of inorganic pollutants (Ioannidis & Zouboulis, 2003).

In the preceding article, it was shown that several weeks of annealing were required to stabilize the lead partitioning $k_{\rm Pb}(A^{\rm I}/A^{\rm II})$ over the large cation–acceptor sites $A^{\rm I}$ and $A^{\rm II}$ of $(Pb_xCa_{10-x})(VO_4)_6(F_{1-2y}O_y\square_y)_2$, $0 < x < 9$ and $0 < y < 0.5$, vanadinites. It was demonstrated that the $A^{\rm I}O_6$ metaprism twist angle (φ) is a sensitive probe for disequilibrium and that it tracks $k_{\rm Pb}$ and the c/a ratio. In this paper we describe the

Table 1
Unit-cell and atomic parameters for $(Pb_xCa_{10-x})(VO_4)_6(F_{1-2y}O_y\square_y)_2$, $0 < x < 7$, $010 < y < 047$.

$x = 0$ is strictly monoclinic. x, y of $A^I = \frac{1}{2}, \frac{2}{3}$; x, y, z of F/O = 0,0, $\frac{1}{4}$; and z of Ca2, V, O1 and O2 = $\frac{1}{4}$.

	Single phase		Miscibility gap				Single phase			
			1.61 (average)		2.78 (average)					
x	0	0.57	1.33	3.01	3.06	1.76	3.82	4.42	5.55	7.00
Wt %	100	100	83.3	16.7	79.0	21.0	100	100	100	100
R_{wp}†	0.289	0.239	0.213	0.213	0.201	0.201	0.183	0.17	0.176	0.21
S_{wp}	1.2	1.2	1.1	1.1	1.2	1.2	1.1	1.1	1.2	1.3
R_b	0.070	0.051	0.052	0.066	0.046	0.051	0.044	0.056	0.071	0.091
a (Å)	9.7371 (1)	9.7835 (3)	9.8208 (6)	9.9175 (7)	9.9174 (4)	9.8441 (5)	9.9559 (2)	9.9856 (2)	10.0233 (2)	10.0531 (1)
c (Å)	7.0063 (1)	7.0318 (2)	7.0521 (5)	7.1154 (6)	7.1199 (3)	7.0635 (5)	7.1508 (2)	7.1825 (1)	7.2410 (2)	7.3033 (1)
V (Å^3)	575.29 (1)	582.89 (3)	589.04 (8)	606.09 (10)	606.47 (5)	592.80 (7)	613.83 (3)	620.24 (2)	630.01 (3)	639.23 (2)
N(Ca1)‡	1	0.97 (2)	0.92 (3)	0.79 (11)	0.82 (4)	0.9 (1)	0.78 (3)	0.78 (3)	0.69 (4)	0.58 (7)
N(Ca2)	1	0.93 (2)	0.84 (3)	0.64 (14)	0.61 (5)	0.78 (12)	0.51 (4)	0.41 (5)	0.28 (6)	0.12 (10)
$k_{Pb}(A^I/A^{II})$§	–	0.31	0.34	0.38	0.30	0.31	0.30	0.25	0.29	0.32
$z(A1)$	0.9993 (5)	0.0019 (8)	0.0037 (10)	0.0005 (50)	0.0068 (12)	0.0071 (45)	0.00490 (9)	0.0087 (9)	0.0045 (8)	0.0067 (10)
$B(A1)$	0.61	0.43	0.95	0.93	0.21	0.94	0.91	0.76	1.12	1.17
$x(A2)$‡	0.2431 (3)	0.2434 (3)	0.2437 (4)	0.2495 (11)	0.2432 (3)	0.2450 (14)	0.2454 (2)	0.2434 (2)	0.2431 (2)	0.2453 (3)
$y(A2)$	0.0005 (3)	0.0006 (4)	0.0021 (5)	0.0058 (18)	0.0015 (5)	0.0048 (19)	0.0038 (3)	0.0015 (3)	0.0015 (3)	0.0045 (4)
$B(A2)$	0.50	0.2	0.88	0.78	0.22	1.42	0.9	0.79	1.5	0.69
x(V)	0.3984 (2)	0.3996 (4)	0.4012 (5)	0.4022 (26)	0.4064 (8)	0.4030 (26)	0.4028 (6)	0.4029 (5)	0.4056 (6)	0.4024 (8)
y(V)	0.3702 (2)	0.3714 (4)	0.3717 (5)	0.3784 (24)	0.3790 (7)	0.3800 (27)	0.3766 (5)	0.3763 (5)	0.3810 (6)	0.3720 (8)
B(V)	0.2	0.2	0.6	0.99	0.26	1.78	0.86	0.2	0.84	0.2
x(O1)	0.3181 (8)	0.3209 (10)	0.3178 (14)	0.3180 (56)	0.3280 (19)	0.3232 (58)	0.3280 (14)	0.3288 (15)	0.3402 (16)	0.3637 (26)
y(O1)	0.4918 (7)	0.4937 (10)	0.4891 (13)	0.4932 (64)	0.4975 (20)	0.4995 (57)	0.4977 (15)	0.4981 (14)	0.5079 (16)	0.5205 (23)
x(O2)	0.6018 (8)	0.6018 (11)	0.6036 (16)	0.6022 (72)	0.6045 (23)	0.6050 (70)	0.6020 (17)	0.6028 (18)	0.6007 (19)	0.5982 (28)
y(O2)	0.4720 (8)	0.4739 (11)	0.4721 (16)	0.4662 (63)	0.4797 (19)	0.4739 (65)	0.4728 (15)	0.4806 (15)	0.4842 (16)	0.4528 (24)
x(O3)	0.3352 (6)	0.3323 (7)	0.3371 (9)	0.3227 (36)	0.3427 (15)	0.3452 (36)	0.3407 (11)	0.3378 (9)	0.3481 (10)	0.3437 (12)
y(O3)	0.2464 (6)	0.2458 (7)	0.2513 (10)	0.2738 (45)	0.2597 (15)	0.2541 (35)	0.2573 (11)	0.2537 (10)	0.2477 (11)	0.2555 (12)
z(O3)	0.0559 (7)	0.0590 (9)	0.0577 (13)	0.0480 (38)	0.0603 (14)	0.0612 (48)	0.0592 (11)	0.0628 (11)	0.0769 (12)	0.0678 (14)
N(F/O)	0.90 (5)	0.90 (5)	0.81 (20)	0.79 (84)	0.85 (31)	0.75 (70)	0.73 (23)	0.85 (19)	0.68 (21)	0.53 (29)
φ (°)	22.7	21.7	22.3	23.2	18.5	20.4	19.6	18.5	15.2	11.8

† Agreement measures are $R_{wp} = \left[\sum_i w_i |y_{io} - y_{ci}|^2 / \sum_i w_i y_{io}^2\right]^{1/2}$; $S_{wp} = \left(R_{wp}/R_{exp}\right)^2$; $R_b = \sum_i |I_{ko} - I_{kc}| / \sum_i I_{ko}$. ‡ $N(A^I) = N(\text{Ca1}) + N(\text{Pb1}) = 1$ and $N(A^{II}) = N(\text{Ca2}) + N(\text{Pb2}) = 1$. § $k_{Pb}(A^I/A^{II}) = (2 - 2N(\text{Ca1}))/(3 - 3N(\text{Ca2}))$. Equal partitioning of Pb over A^I and A^{II}; $k_{Pb} = 0.66$.

Rietveld refinement of equilibrated structures and develop a model relating the unit-cell constants to φ, average crystal radii and ultimately to chemical composition.

2. Experimental methods

The idealized vanadinite series $(Pb_xCa_{10-x})(VO_4)_6F_2$ was prepared according to the procedures of Dong & White (2004) with annealing continued at 1073 K for 4 weeks to stabilize the structures. X-ray powder diffraction (XRD) and Rietveld analysis were conducted as described earlier, except that for high lead contents ($x > 5$) 50 wt % diamond powder was introduced into the samples in an effort to minimize the effects of absorption, as initial refinements showed that thermal parameters were high or unstable. However, this procedure did not noticeably improve convergence. Most compositions were refined in $P6_3/m$, although for the calcium endmember a monoclinic distortion was evident (Kreidler & Hummel, 1970) and the subgroup $P2_1/m$ was used.

3. Results

3.1. Phase chemistry and cell constant refinement

The refined unit-cell data are summarized in Table 1. A miscibility gap was observed for $(Pb_xCa_{10-x})(VO_4)_6F_{2\delta}$ with $2 < x < 3$, where a two-phase vanadinite assemblage was observed such that the nominal $x = 2$ material consisted of coexisting $x = 1.33$ and 3.01 structures, while $x = 3$ was composed of $x = 1.76$ and $x = 3.06$ compounds. Inspection of the Rietveld traces clearly differentiates Bragg reflections due to the two phases (Fig. 1). The overall average composition for the phases yields $x = 1.61$ and 2.78 rather than the starting compositions of $x = 2$ and 3, respectively. Indeed, all specimens invariably refined to x less than its nominal value due to the slow loss of PbF_2 during annealing. Volatilization was parti-

Table 2
Unit-cell and atomic parameters for $Ca_{10}(VO_4)_6(F_{0.90}O_{0.05}\square_{0.05})_2$.

a = 9.7370 (3), b = 9.7358 (4), c = 7.00572 (9) Å, β = 120.002 (5)°, V = 575.14 (4) Å^3; space group $P2_1/m$; R_{wp} = 0.286; S_{wp} = 1.2; R_{exp} = 0.240; R_b = 0.058

Site	x	y	z	B (Å^2)	N
Ca1	0.3327 (33)	0.6688 (33)	0.9997 (6)	0.65	1
Ca2	0.2332 (27)	0.9958 (31)	0.25	0.50	1
Ca3	0.9945 (21)	0.2445 (40)	0.25	0.50	1
Ca4	0.7534 (37)	0.7542 (50)	0.25	0.50	1
V1	0.3926 (24)	0.3687 (29)	0.25	0.21	1
V2	0.6319 (28)	0.0303 (27)	0.25	0.21	1
V3	0.9712 (28)	0.5970 (27)	0.25	0.21	1
O1*a*	0.352 (4)	0.520 (5)	0.25	1	1
O1*b*	0.522 (11)	0.827 (8)	0.25	1	1
O1*c*	0.174 (9)	0.693 (11)	0.25	1	1
O2*a*	0.595 (8)	0.476 (8)	0.25	1	1
O2*b*	0.533 (10)	0.135 (11)	0.25	1	1
O2*c*	0.864 (11)	0.393 (11)	0.25	1	1
O3*a*	0.340 (7)	0.242 (8)	0.059 (10)	1	1
O3*b*	0.753 (7)	0.079 (6)	0.055 (9)	1	1
O3*c*	0.910 (8)	0.659 (8)	0.057 (10)	1	1
F/O	0.012 (11)	0.999 (16)	0.25	1	0.95

cularly significant for $x \geq 8$ and vanadinite proved increasingly difficult to prepare with yields of 91, 47 and 0 wt % for x = 8, 9 and 10, respectively.

Unit-cell constants expanded as lead-replaced calcium (Fig. 2) with the observance of Vergard's Law in two compositional segments described by

$$a = 9.737 + 0.0587x \quad \text{for } 0 < x < \sim 5$$
$$a = 10.108 - 0.0189(1 - x) \quad \text{for } \sim 5 < x < 10$$

and

$$c = 7.006 + 0.0382x \quad \text{for } 0 < x < \sim 5$$
$$c = 7.420 - 0.0399(1 - x) \quad \text{for } \sim 5 < x < 10.$$

3.2. Structure refinement $P6_3/m$ vanadinite

The refined structural parameters for vanadinites with $0 < x < 7$ are collated in Tables 1 and 2. As x increased from 0 to 7 average bond lengths of $A^{I}O_6$ and $A^{II}O_6F$ increased as the lead content was raised and the metaprism volume increased (Tables 3 and 4). However, at x = 5.55 the metaprism contracted while the A^{II} polyhedra expanded. As anticipated the A^{I} site is smaller than A^{II} with lead preferentially occupying A^{II} (Bigi *et al.*, 1989; Andres-Verges *et al.*, 1983). The VO_4 tetrahedra were less variable.

The occupancy of the X anion site fell progressively as the lead content increased in a manner consistent with the replacement

$$2F^- \rightarrow O^{2-}.$$

The limiting compositions of fluorine and oxyvanadinite are $(Pb_xCa_{10-x})(VO_4)_6F_2$ and $(Pb_xCa_{10-x})(VO_4)_6O$ with near endmembers observed for x = 0 and x = 7, respectively. The trend in X site occupancy is illustrated in Fig. 3 and varies linearly for $0 < x < 7$. For x = 8, nine X-site occupations < 0.5 were refined, however the crystallinity of such apatites was

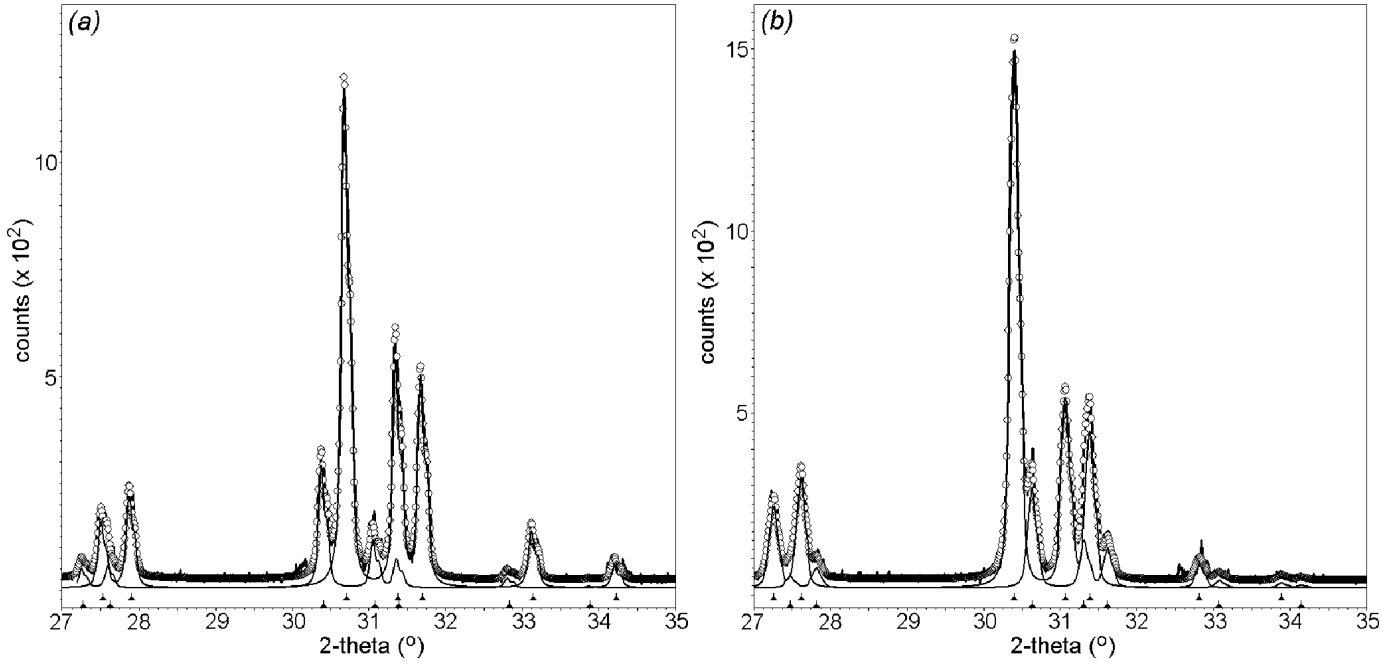

Figure 1
Final fit between calculated and experimental diffraction profiles for $(Pb_xCa_{10-x})(VO_4)_6(F/O)_{2\delta}$ with (*a*) nominal x = 2 and (*b*) x = 3. At these compositions immiscibility causes fractionation such that in (*a*) the co-existing phases have x = 1.33 (upper Bragg markers) and 3.01 (lower), and crystal chemical formulae $[Ca_{3.66}Pb_{0.34}][Ca_{3.02}Pb_{2.98}](VO_4)_6(F_{1.22}O_{0.20})$ and $[Ca_{3.16}Pb_{0.84}][Ca_{3.82}Pb_{2.18}](VO_4)_6(F_{1.01}O_{0.25})$, respectively, and in (*b*) x = 1.76 (lower) and 3.06 (upper), and formulae $[Ca_{3.58}Pb_{0.42}][Ca_{4.66}Pb_{1.34}](VO_4)_6(F_{1.18}O_{0.21})$ and $[Ca_{3.30}Pb_{0.70}][Ca_{3.64}Pb_{2.36}](VO_4)_6(F_{1.40}O_{0.30})$, respectively.

Table 3
Selected bond lengths (Å) for $(Pb_xCa_{10-x})(VO_4)_6(F_{1-2y}O_y\square_y)_2$ apatites as a function of composition.

Composition: x	0.57	1.33	1.76	3.01	3.06	3.82	4.42	5.55	7.00
A^I—O1 × 3	2.391 (8)	2.412 (11)	2.345 (48)	2.423 (54)	2.391 (17)	2.411 (12)	2.401 (12)	2.409 (13)	2.420 (21)
A^I—O2 × 3	2.511 (10)	2.507 (15)	2.534 (61)	2.484 (64)	2.593 (19)	2.561 (14)	2.638 (15)	2.668 (16)	2.502 (22)
Average	**2.451**	**2.459**	**2.439**	**2.453**	**2.492**	**2.486**	**2.519**	**2.539**	**2.461**
A^IO_6 volume	15.84	15.96	15.84	15.34	16.43	16.24	16.99	16.96	14.34
A^{II}—O1	2.863 (9)	2.853 (12)	2.949 (47)	2.914 (49)	2.975 (16)	2.998 (12)	2.997 (12)	3.116 (13)	3.211 (12)
A^{II}—O2	2.399 (10)	2.421 (14)	2.400 (55)	2.445 (55)	2.382 (16)	2.434 (13)	2.392 (13)	2.376 (14)	2.630 (21)
A^{II}—O3 × 2	2.495 (8)	2.535 (10)	2.521 (36)	2.780 (45)	2.610 (14)	2.596 (10)	2.582 (10)	2.485 (10)	2.679 (15)
A^{II}—O3 × 2	2.338 (7)	2.350 (10)	2.411 (35)	2.231 (30)	2.400 (12)	2.399 (9)	2.424 (9)	2.587 (9)	2.386 (13)
A^{II}—F	2.379 (4)	2.383 (4)	2.389 (17)	2.446 (14)	2.406 (4)	2.425 (3)	2.424 (3)	2.430 (3)	2.444 (3)
Average	**2.473**	**2.490**	**2.515**	**2.547**	**2.540**	**2.550**	**2.546**	**2.581**	**2.631**
V—O1	1.717 (13)	1.715 (18)	1.711 (76)	1.716 (83)	1.703 (26)	1.705 (19)	1.711 (19)	1.698 (21)	1.720 (31)
V—O2	1.712 (10)	1.722 (15)	1.723 (66)	1.722 (72)	1.704 (22)	1.718 (16)	1.729 (16)	1.695 (18)	1.714 (28)
V—O3 × 2	1.714 (6)	1.700 (10)	1.712 (35)	1.716 (31)	1.696 (12)	1.709 (9)	1.713 (9)	1.709 (10)	1.727 (13)
Average	**1.715**	**1.709**	**1.715**	**1.718**	**1.708**	**1.710**	**1.717**	**1.702**	**1.722**

noticeably degraded as evidenced by peak-broadening and $Ca_3(VO_4)_2$ was present as a secondary phase, limiting the reliability of these data. Nonetheless, it would appear that excessive loss of fluorine from the X site without concomitant oxygen replenishment contributes to the destabilization of vanadinite.

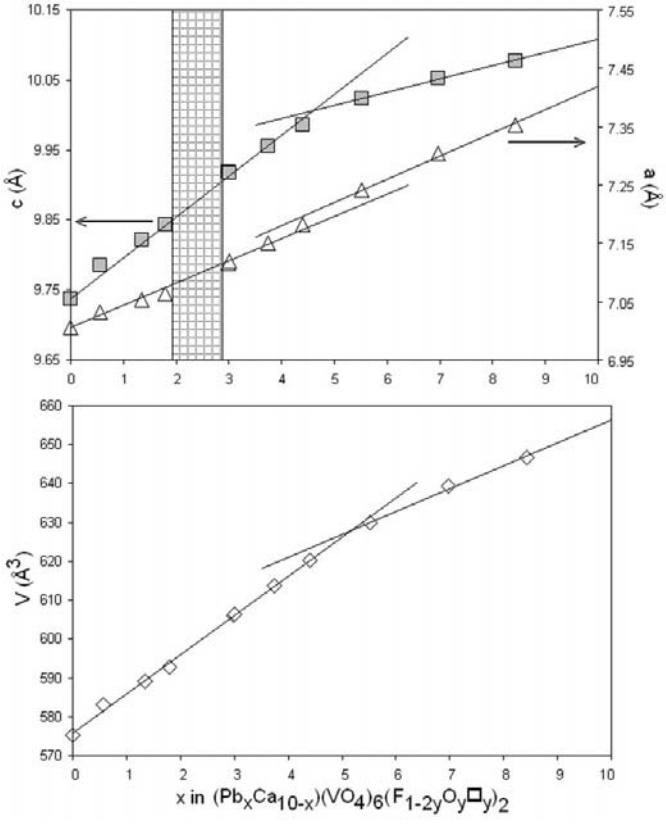

Figure 2
Unit-cell parameter trends after annealing for 4 weeks at 1073 K. A miscibility gap appears for $\sim 2 < x < \sim 3$. Error bars are smaller than the graph symbols (see Table 1). This figure should be compared with Fig. 1 in Dong & White (2004) that shows data for vanadinite in disequilibrium.

Lead partitioning was relatively constant with $k_{Pb}(A^I/A^{II}) = [2 - 2N(Ca1)]/[3 - 3N(Ca2)]$ staying close to an average value of 0.31 for most compositions (Fig. 4). With equal partitioning $k_{Pb} = 0.66$ would lead to the proportional substitution of calcium by lead such that

$$4[A]^I + 6[A]^{II} = [((4 - 0.4x)Ca1)(0.4xPb1)]^I + [((6 - 0.6x)Ca2)(0.6xPb2)]^{II}.$$

The present refinements suggest the thermodynamically preferred mechanism for substitution (with $k_{Pb} = 0.33$) is

$$4[A]^I + 6[A]^{II} = [((4 - 0.25x)Ca1)(0.25xPb1)]^I + [((6 - 0.75x)Ca2)(0.75xPb2)]^{II}.$$

Using this idealized rate of lead replacement, the A^{II} site will be completely filled for the composition $(Pb_8Ca_2)(VO_4)_6(F,O)_{2\delta} \simeq [Ca_2Pb_2][Pb_6](VO_4)_6(F,O)_{2\delta}$, after which lead must displace calcium in the smaller A^I site (Table 5).

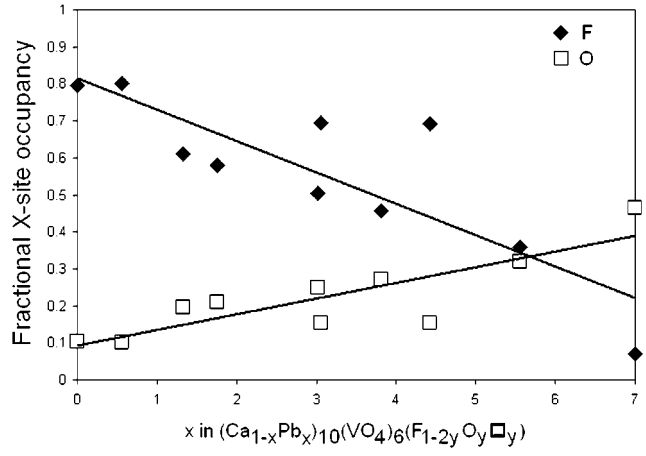

Figure 3
Variation in fluorine and oxygen X-site occupancy F as a function of composition (x).

Table 4
Selected bond lengths (Å) for $Ca_{10}(VO_4)_6(F_{1.90}O_{0.05}\square_{0.05})$.

Ca1—O1*a*	2.342 (28)	Ca2—O1*c*	2.702 (84)	V1—O1*a*	1.705 (42)
Ca1—O1*b*	2.451 (39)	Ca2—O2*b*	2.531 (83)	V1—O2*a*	1.712 (60)
Ca1—O1*c*	2.428 (61)	Ca2—O3*a* × 2	2.470 (51)	V1—O3*a* × 2	1.715 (53)
Ca1—O2*a*	2.556 (64)	Ca2—O3*b* × 2	2.281 (37)	Average	**1.711**
Ca1—O2*b*	2.434 (44)	Ca2—F	2.162 (92)		
Ca1—O2*c*	2.433 (58)	Average	**2.414**	V2—O1*b*	1.713 (59)
Average	**2.441**			V2—O2*b*	1.715 (110)
Ca^IO_6 volume	15.52	Ca3—O1*a*	3.162 (26)	V2—O3*b* × 2	1.712 (36)
		Ca3—O2*c*	2.361 (110)	Average	**1.713**
		Ca3—O3*b* × 2	2.491 (30)		
		Ca3—O3*c* × 2	2.343 (52)	V3—O1*c*	1.709 (62)
		Ca3—F	2.487 (110)	V3—O2*c*	1.717 (76)
		Average	**2.525**	V3—O3*c* × 2	1.711 (59)
				Average	**1.712**
		Ca4—O1*b*	2.683 (95)		
		Ca4—O2*a*	2.351 (59)		
		Ca4—O3*a* × 2	2.358 (58)		
		Ca4—O3*c* × 2	2.531 (72)		
		Ca4—F	2.453 (64)		
		Average	**2.466**		

For hexagonal apatites the A^IO_6 metaprism twist angle ranges from $21._7$ to $11._8^\circ$ for $0.57 < x < 7.0$, respectively. As the lead content of the A^{II} site increases the apatite channel expands through reduction of φ to accommodate the larger ion. The structure drawings of $[Pb_{3.66}Ca_{0.34}][Pb_{5.02}Ca_{0.98}](VO_4)_6(F_{1.22}O_{0.40}\square_{0.40})$ and $[Pb_{2.30}Ca_{1.70}][Pb_{0.70}Ca_{5.30}](VO_4)_6(F_{0.142}O_{0.94}\square_{0.94})$ illustrate the cooperative twisting of the metaprisms (Fig. 5).

3.3. Structure refinement $P2_1/m$ vanadinite

$Ca_{10}(VO_4)_6(F_{1.80}O_{0.10}\square_{0.10})$ vanadinite was monoclinic, yielding the refined parameters given in Table 2. Clear splitting of the reflections, first observed by Kreidler & Hummel (1970), was evident, with R_b for the monoclinic cell (0.058) significantly lower than that obtained using the hexagonal cell (0.070) (Table 1). The crystal chemical formula for $P2_1/m$ is $[Ca1^I]_4[Ca2^{II}]_2[Ca3^{II}]_2[Ca4^{II}]_2[V1O_4]_2[V2O_4]_2[V3O_4]_2(F_{1.80}O_{0.05})$. The bond lengths show slight departures from that expected for hexagonal symmetry (Table 4). With the reduction of symmetry the O atoms move freely on the (001) plane and therefore the CaO_6 metaprism is defined by three independent φ, ranging from $12._8$ to $26._7^\circ$ with an average value of $21._5^\circ$ (Fig. 6). This compares with $22._7^\circ$ when the refinement is forced to $P6_3/m$ symmetry.

4. Discussion

4.1. Twist angle modelling

Fluoro-vanadinites can be regarded as derivatives of the planar triangular anion nets between which cations are periodically inserted to form trigonal prisms (A^IO_6), octahedra ($A^{II}O_5X$) or tetrahedra (BO_4) – in this instance $(Ca,Pb)O_6$, $(Ca,Pb)O_5F$ and VO_4 (White & Dong, 2003). For this description trigonal prisms are included in structure drawings, in addition to the illustration of tetrahedra (as in Figs. 5 and 6), to more readily monitor systematic changes in crystal chemistry and topology. It has been noted previously that the A^IO_6 trigonal prisms are twisted by an angle φ to form metaprisms such that the degree of rotation varies inversely with the average ionic/crystal radius of the unit-cell contents (White & Dong, 2003).

As apatite topology can be derived from the twisting of regular triangular nets, and the A^IO_6 and BO_4 polyhedra are corner-connected, it is feasible to predict and model the relative changes in unit-cell parameters as a function of experimentally derived φ's. Moreover, because φ varies as a function of composition, a scalar derived from the average A^I—O bond length can be incorporated to adjust the geometry in an absolute sense. From these purely geometrical (Fig. 7) and crystal chemical considerations, it can be shown that the basal unit-cell dimension a is related to φ and the equilateral triangle edge t such that

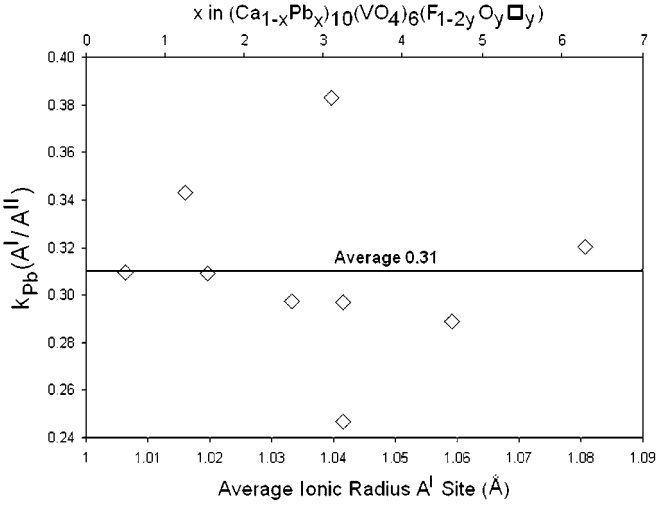

Figure 4
Variation in the lead partitioning coefficient (k_{Pb}) as a function of composition (x) and the average ionic radius of A^I. The two outlying points arise from the minor phases in the two-phase region.

Table 5
A-metal partitioning in $(Pb_xCa_{10-x})(VO_4)_6(F,O)_{2\delta}$ vanadinite for k_{Pb} = 0.66 and 0.33 as a function of composition (x).

	k_{Pb} = 0.66				k_{Pb} = 0.33			
	A^I		A^{II}		A^I		A^{II}	
x	Ca1	Pb1	Ca2	Pb2	Ca1	Pb1	Ca2	Pb2
0	4	0	6	0	4	0	6	0
1	3.6	0.4	5.4	0.6	3.75	0.25	5.25	0.75
2	3.2	0.8	4.8	1.2	3.5	0.5	4.5	1.5
3	2.8	1.2	4.2	1.8	3.25	0.75	3.75	2.25
4	2.4	1.6	3.6	2.4	3	1	3	3
5	2	2	3	3	2.75	1.25	2.25	3.75
6	1.6	2.4	2.4	3.6	2.5	1.5	1.5	4.5
7	1.2	2.8	1.8	4.2	2.25	1.75	0.75	5.25
8	0.8	3.2	1.2	4.8	2	2	0	6
9	0.4	3.6	0.6	5.4	1	3	0	6
10	0	4	0	6	0	4	0	6

$$a = t\left[13 - 28\sin^2\left(\frac{\varphi}{4}\right) + 16\sin^4\left(\frac{\varphi}{4}\right)\right]^{1/2},$$

where $t = 2.729 + 0.017x$ and x is the stoichiometric parameter in $(Pb_xCa_{10-x})(VO_4)_6(F_{2-2y}O_y)$. The compositional adjustment factor for t is derived from the increase in ionic radii for Ca^{2+} (IR = 1.18 Å) and Pb^{2+} (IR = 1.35 Å) divided by the total A-cation formula content, *i.e.* (1.35 − 1.18)/10 = 0.017 Å. As the B cation is fixed, no adjustment is made for its ionic radius.

Similarly, the c cell parameter can be related to φ as

$$c = 2\left[h_{\varphi=0}^2 - \frac{4t^2}{3}\sin^2\left(\frac{\varphi}{2}\right)\right],$$

where the prism height $h_{\varphi=0} = 3.555 + 0.017x$ at $\varphi = 0^\circ$.

Table 6
Calculated cell parameters a_{calc} and c_{cal} derived from the rotation and collapse of a regular triangular anion net as a function of observed twist angles (φ_{exp}) for $(Pb_xCa_{10-x})(VO_4)_6(F_{1-2y}O_y\square_y)_2$.

x	φ_{exp} (°)	t (Å)	$h_{\varphi=0}$ (Å)	a_{calc} (Å)	c_{calc} (Å)
0	22.7	2.729	3.555	9.74	7.00
0.57	21.7	2.739	3.565	9.78	7.03
1.33	22.4	2.752	3.578	9.82	7.04
1.76	23.3	2.759	3.607	9.84	7.03
3.01	20.4	2.780	3.585	9.94	7.11
3.06	18.5	2.781	3.607	9.96	7.12
3.82	19.6	2.794	3.620	9.99	7.13
4.42	18.5	2.804	3.630	10.04	7.16
5.55	15.2	2.823	3.649	10.13	7.23
7.00	11.8	2.848	3.674	10.24	7.30

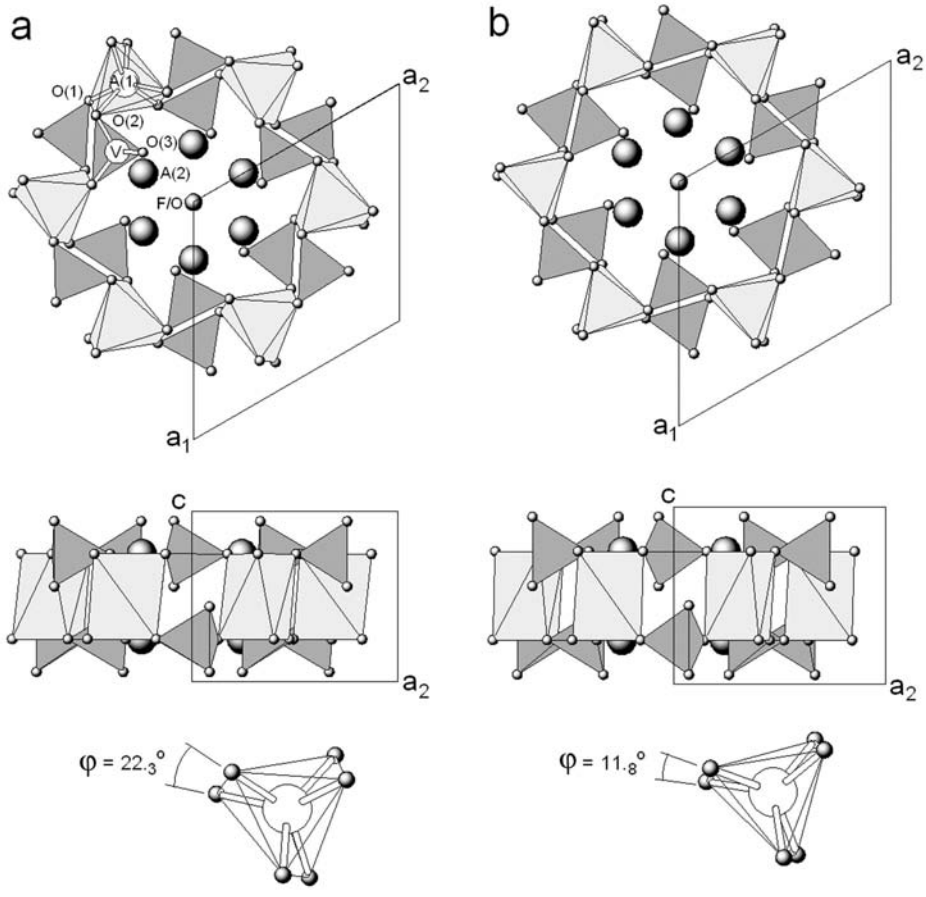

Figure 5
Refined structures of (*a*) $[Ca_{3.66}Pb_{0.34}][Ca_{5.02}Pb_{0.98}](VO_4)_6(F_{1.22}O_{0.20})$ and (*b*) $[Ca_{2.30}Pb_{1.70}]$-$[Ca_{0.70}Pb_{5.30}](VO_4)_6(F_{0.14}O_{0.47})$ have the average cell-content crystal radii of 1.124 and 1.146 Å, and corresponding φ values of 22.3 and 11.8°, respectively. The upper part of the figure shows the structures projected down [0001]. The A^IO_6 metaprisms and VO_4 tetrahedra are emphasized as this representation highlights the cooperative movements of these polyhedra. The lower portion of the drawing shows the A^IO_6 metaprisms in more detail, including the twist angle φ. Three more distant O atoms, that for clarity are not illustrated, cap each metaprism.

Using these simple relationships, and taking the experimentally observed metaprism twist angles (φ_{exp}) and composition (x) as input, reasonable agreement with refined cell constants is obtained across the solid solution series (Table 6, Fig. 8). For the c parameter, agreement was satisfactory across the entire range, however, for the a parameter agreement degraded at a smaller twist angle, which corresponds to higher lead contents, such that the experimental value exceeded the calculated value. This effect arises because the precision of tracking lattice trends will be reduced by the distortion of the triangular net (in $P6_3/m$ the upper and lower triangles of the metaprisms need not be the same size) and this is not included in the modelling. In lead-rich samples a mismatch of the triangular faces, determined by the O1—O1 and O2—O2 distances, is related to the presence of stereochemically active electron lone pairs. Such distortions have been observed in phosphate analogues, where the difference in PbO_6 metaprism faces for $Pb_{10}(PO_4)_6F_2$ exceeds 19%, while those calcium, cadmium and strontium analogues do not differ by more

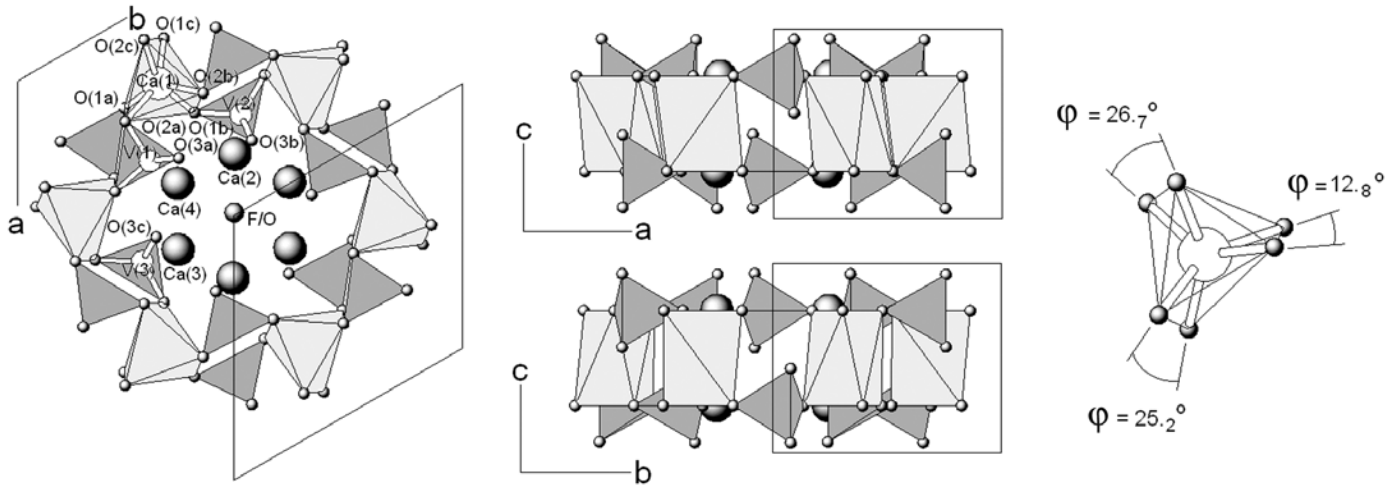

Figure 6
Structure drawing of the monoclinic vanadinite $Ca_{10}(VO_4)_6(F_{0.90}O_{0.05}\square_{0.05})_2$.

than 7% and are frequently much less (Table 7). It is anticipated that the geometrical unit-cell modelling approach would show better agreement for systems where less distorted metaprisms are formed, such as in a $Ca_{10}(PO_4)_6F_2$–$Sr_{10}(PO_4)_6F_2$ join. Further improvement in modelling may be achieved by integrating this purely geometrical approach with artificial neural network methods under development (Wu *et al.*, 2004) to predict apatite lattice constants.

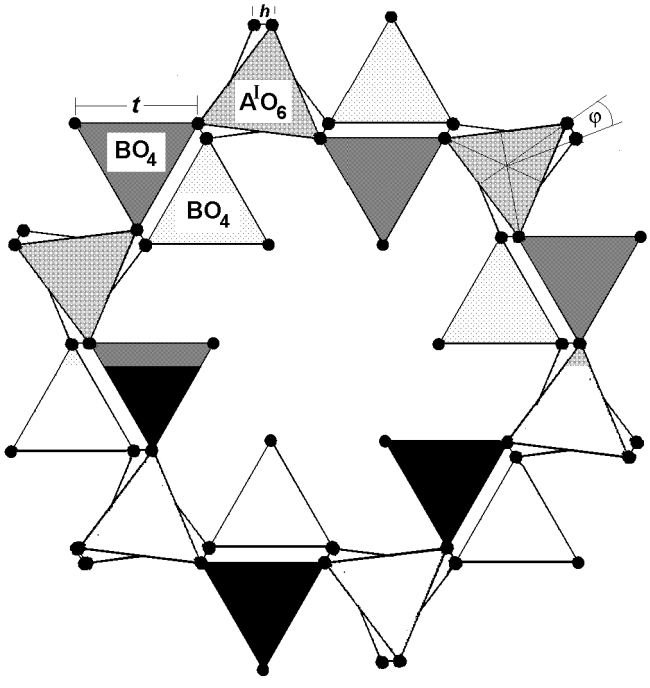

Figure 7
Construction used for the derivation of equations for the calculation of cell parameters from overlapping triangular anion nets at different heights. The triangle edge length (t), metaprism height (h) and twist angle (φ) are shown. This idealized representation should be compared with the real structures in Fig. 5.

Table 7
Metaprism bond lengths (Å) in O1—O1 and O2—O2 and triangular face distortions in selected phosphate apatites.

	O1—O1	O2—O2	% difference	Reference
$Sr_{10}(PO_4)_6(OH)_2$	3.127	3.134	0.2	Sudarsanan & Young (1972)
$Pb_{10}(PO_4)_6F_2$	2.954	3.522	19.2	Kim *et al.* (2000)
$Ca_{10}(PO_4)_6F_2$	2.895	3.011	4.0	Sudarsanan *et al.* (1972)
$Cd_{10}(PO_4)_6(OH)_2$	2.85	3.044	6.8	Hata *et al.* (1978)

4.2. Twist angle and chemistry

There is an inverse linear correlation between the twist angle and the average ionic radius of the A^I site and the average crystal radius of the entire cell contents (Table 6). This arises from two sources. First, as the A^I cation radius decreases, shortening of the A^I—O distance can be achieved through increasing the twist angle. Second, as the contents of the channels (A^{II} and X anions) decrease in size and/or occupancy the channels must collapse through an increase in twist angle. These trends are summarized for Ca—Pb vanadinite, calcium and lead apatites (Table 8, Fig. 9).

Although this is the first investigation of Ca/Pb substitution in vanadinite apatite, several comparative analyses have appeared for the hydroxy-phosphate analogue $(Pb_xCa_{10-x})(PO_4)_6OH$. Earlier studies of phosphate apatites indicated that cell parameters varied in accordance with Vergard's Law (*e.g.* Narasaraju *et al.*, 1972), but more recent research (*e.g.* Andres-Verges *et al.*, 1983) has shown non-linear dilation, with distinct discontinuities. These were scrutinized by Bigi *et al.* (1989) who confirmed earlier speculation that partitioning over the A^I and A^{II} strongly favoured the entry of lead into the latter site. In these experiments compositions having x near 0.20, 0.45 and 0.80 yielded partitioning coefficients $k_{Pb}(A^I/A^{II})$ of 0.05, 0.05 and 0.33, respectively, by X-ray refinement. As these apatites were fired at 1173 K overnight,

Table 8
Variation in the metaprism twist angle (φ) of vanadate and phosphate apatite as a function of average crystal radius.

For $A_{10}(BO_4)_6X_2$ apatites the average crystal radius (CR_{av}) was calculated with the data extracted from Shannon & Prewitt (1970): Ca^{IX} 1.18; Ca^{VI} 1.00; Pb^{IX} 1.29; Pb^{VI} 1.19; P^{IV} 0.17; V^{IV} 0.355; F^{VI} 1.33; OH^{VI} 1.37 – as follows, $CR_{av} = [(CR_{A^I} \times 4) + (CR_{A^{II}} \times 6) + (CR_B \times 6) + (CR_O \times 24) + (CR_X \times \text{occupancy} \times 2)]/42$.

Composition (this study)	Twist angle (φ)	CR average (Å)
$[Ca_{3.86}Pb_{0.14}][Ca_{5.56}Pb_{0.44}](VO_4)_6(F_{1.60}O_{0.10})$	21.7	1.122
$[Ca_{3.66}Pb_{0.34}][Ca_{5.02}Pb_{0.98}](VO_4)_6(F_{1.22}O_{0.20})$	22.3	1.124
$[Ca_{3.58}Pb_{0.42}][Ca_{4.66}Pb_{1.34}](VO_4)_6(F_{1.18}O_{0.21})$	23.3	1.131
$[Ca_{3.16}Pb_{0.84}][Ca_{3.82}Pb_{2.18}](VO_4)_6(F_{1.01}O_{0.25})$	20.4	1.126
$[Ca_{3.30}Pb_{0.70}][Ca_{3.64}Pb_{2.36}](VO_4)_6(F_{1.40}O_{0.30})$	18.5	1.132
$[Ca_{3.12}Pb_{0.88}][Ca_{3.06}Pb_{2.94}](VO_4)_6(F_{0.92}O_{0.27})$	19.6	1.134
$[Ca_{3.12}Pb_{0.88}][Ca_{2.46}Pb_{3.54}](VO_4)_6(F_{1.40}O_{0.20})$	18.5	1.138
$[Ca_{2.76}Pb_{1.24}][Ca_{1.70}Pb_{4.30}](VO_4)_6(F_{0.72}O_{0.32})$	15.2	1.141
$[Ca_{2.30}Pb_{1.70}][Ca_{0.70}Pb_{5.30}](VO_4)_6(F_{0.14}O_{0.47})$	11.8	1.146

Ca apatites				Pb apatites			
Composition	φ (°)	CR average (Å)	Reference	Composition	φ (°)	CR average (Å)	Reference
$Ca_{10}(PO_4)_6F_2$	23.3	1.143	Sudarsanan *et al.* (1972)	$Pb_{10}(PO_4)_6F_2$	23.5	1.185	Kim *et al.* (2000)
$Ca_{10}(PO_4)_6OH_2$	23.2	1.146	Kim *et al.* (2000)	$Pb_{10}(PO_4)_6OH_2$	26.7	1.189	Kim *et al.* (2000)
$Ca_{10}(PO_4)_6Cl_2$	19.1	1.166	Kim *et al.* (2000)	$Pb_{10}(PO_4)_6Cl_2$	17.6	1.208	Kim *et al.* (2000)
$Ca_{10}(CrO_4)_6OH_2$	17.8	1.171	Wilhelmi & Jonsson (1965)	$Pb_{10}(VO_4)_6Cl_2$	17.5	1.235	Dai & Hughes (1989)
$Ca_{10}(PO_4)_6Br_2$	16.3	1.173	Kim *et al.* (2000)	$Pb_{10}(VO_4)_6I_2$	16.7	1.253	Audubert *et al.* (1999)
$Ca_{10}(AsO_4)_6Cl_2$	13.0	1.189	Wardojo & Hwu (1996)				
$Ca_4Pb_6(AsO_4)_6Cl_2$	5.2	1.214	Rouse *et al.* (1984)				

and the spread of k_{Pb} is large it might be expected that some samples have not attained equilibrium, although the possibility that phosphates may equilibrate more rapidly than the vanadinites should not be excluded. Clearly the approach to equilibrium will be strongly influenced by preparative conditions. While Bigi *et al.* used solid-state methods, the recent study of $(Pb_xCa_{10-x})(PO_4)_6(OH)_2$ by Yasukawa *et al.* (2002) employed co-precipitation and found discontinuity in lattice parameters at $x \simeq 1$ and 8. It is clear that for apatites containing mixed A cations some care is needed to establish whether the lattice parameters and the partitioning coefficients represent transient or thermodynamically stable states. Even more complex behaviours can be expected for ternary substitutions in $(Pb,Cd,Ca)_{10}(PO_4)_6(OH)_2$ apatites where the replacement of calcium reportedly leads to dilation of a and contraction of c (Mahapatra *et al.*, 1995). In this case, stable partitioning is likely to be achieved more slowly and extended A-cation ordering may lead to a reduction in symmetry (*e.g.* to

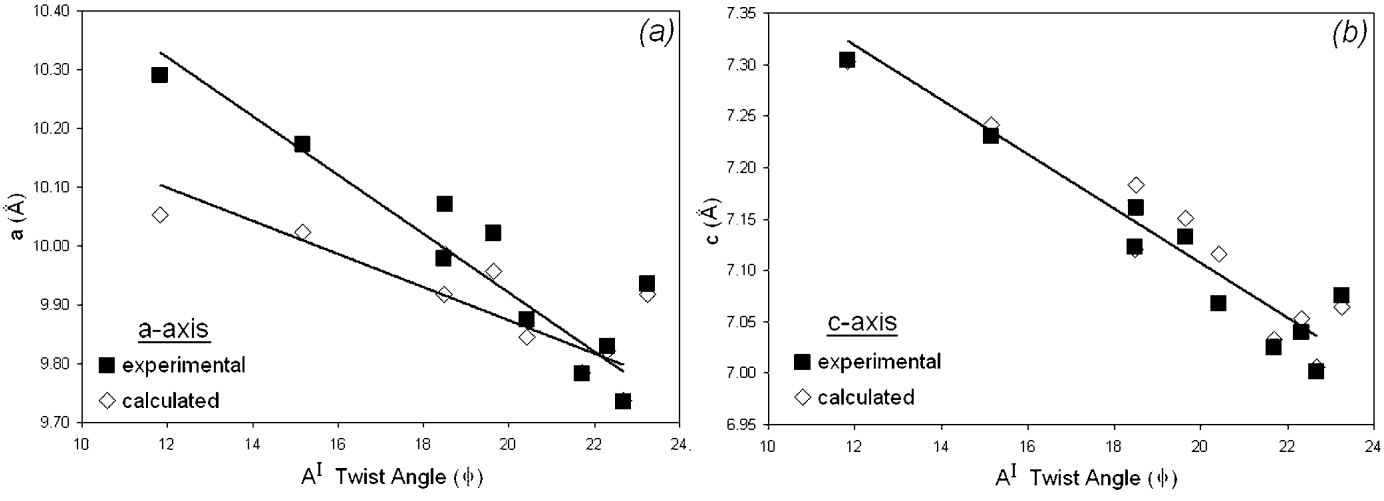

Figure 8
Comparison of observed and calculated (*a*) *a* cell edges and (*b*) *c* cell edges as a function of φ for $(Pb_xCa_{10-x})(VO_4)_6(F,O)_{2\delta}$, $0 < x < 7$. The calculated parameters were obtained from the twist angles (φ_{exp}) derived from Rietveld refinement. The absolute values are listed in Tables 1 and 6.

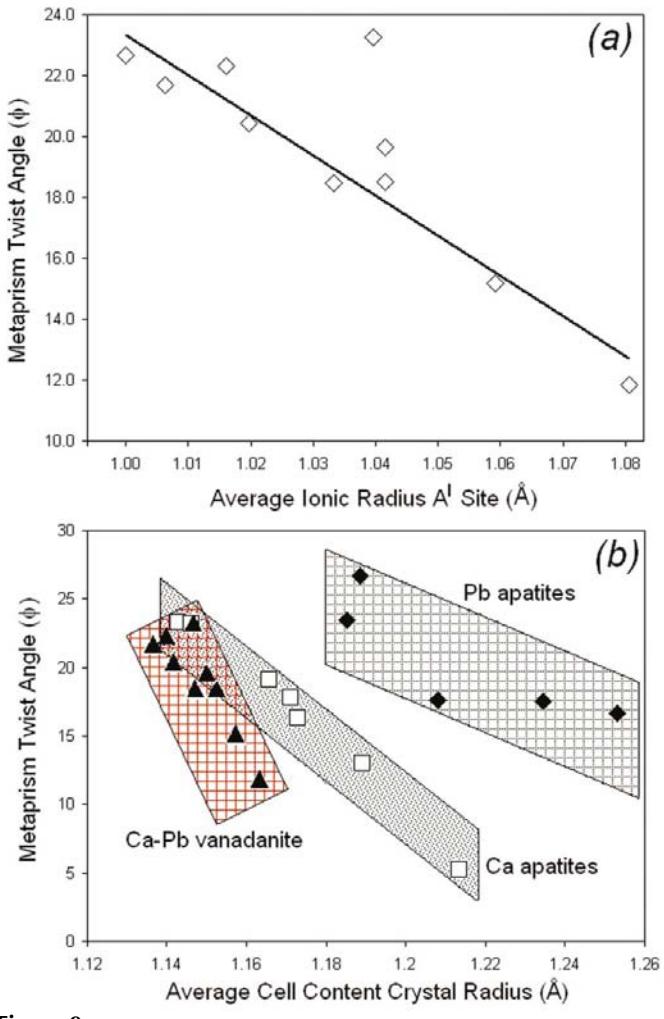

Figure 9
(*a*) Correlation of the $A^{I}O_6$ metaprism twist angle (φ) as refined from Rietveld analysis with the average effective ionic radius of A^{I}. Outlying values arise from minor apatite components in the region of the miscibility gap. Absolute values are collected in Table 1. (*b*) Inverse correlation of the metaprism twist angle (φ) of $A^{I}O_6$ and the average cell content crystal radii for a range of apatites. As the average radius increases, the apatite channel fills and expands through reduction of φ.

$P6_3$). A recent study by Kim *et al.* (2004) has shown that in $A_{10}(P_{1-x}BO_4)_6Cl_2$ apatites, B = Cr, V, rapid equilibration is only possible for near end-members.

5. Conclusions

$(Pb_xCa_{10-x})(VO_4)_6F_2$ apatites prepared at 1073 K in air adopt the $P6_3/m$ apatite structure for all compositions, except the calcium end-member where monoclinic $P2_1/m$ is observed. A miscibility gap is evident for $2 < x < 3$, where dissociation into coexisting vanadinites is observed. The partitioning of lead over the A-sites is relatively constant with $k_{Pb} \simeq 0.33$ and always favouring entry to the larger A^{II} site. Beyond $x = 7$, losses of lead and fluorine prevented the crystallization of single-phase vanadinite. The kinetics for attaining equilibrium are quite slow and several weeks annealing near the melting point are required to stabilize the partitioning coefficient.

Unit-cell data can be modelled using a geometrical approach in which the apatites are derived from regular triangular anion nets. The calculation of ideal cell edges from the observed $A^{I}O_6$ metaprism twist angle φ proves to be a sensitive probe for recognizing the members of a solid-solution series that are far from equilibrium and, in the case of lead, also reflects the presence of stereochemically active lone-pair electrons. It may also be a useful indicator of deviations from $P6_3/m$ symmetry.

This work was supported through A*STAR Grant 012 105 0123.

References

Andres-Verges, M., Higes-Rolando, F. J., Valenzuela-Calahorro, C. & Gonzalez-Diaz, P. F. (1983). *Spectrochim. Acta Part A*, **39**, 1077–1082.
Audubert, F., Savariault, J.-M. & Lacout, J.-L. (1999). *Acta Cryst.* C**55**, 271–273.
Bigi, A., Ripamonti, A., Brückner, S., Gazzano, M., Roveri, N. & Thomas, S. A. (1989). *Acta Cryst.* B**45**, 247–251.
Dai, Y.-S. & Hughes, J. M. (1989). *Can. Mineral.* **27**, 189–192.
Dong, Z. L. & White, T. J. (2004). *Acta Cryst.* B**60**, 138–145.
Hata, M., Okada, K., Iwai, S., Akao, M. & Aoki, H. (1978). *Acta Cryst.* B**34**, 3062–3064.
Ioannidis, T. A. & Zouboulis, A. I. (2003). *J. Hazard. Mater. B*, **97**, 173–191.
Kim, J. Y., Dong, Z. L. & White, T. J. (2004). Submitted for publication.
Kim, J. Y., Fenton, R. R., Hunter, B. A. & Kennedy, B. J. (2000). *Aust. J. Chem.* **53**, 679–686.
Kreidler, E. R. & Hummel, F. A. (1970). *Am. Mineral.* **55**, 170–184.
Mahapatra, P. P., Sarangi, D. S. & Mishra, B. (1995). *J. Solid State Chem.* **116**, 8–14.
Narasaraju, T. S. B., Singh, R. P. & Rao, V. L. N. (1972). *J. Inorg. Nucl. Chem.* **34**, 2072–2074.
Rouse, R. C., Dunn, P. J. & Peacor, D. R. (1984). *Am. Mineral.* **89**, 920–927.
Shannon, R. D. & Prewitt, C. T. (1970). *Acta Cryst.* B**26**, 1046–1048.
Sudarsanan, K., Mackie, P. E. & Young, R. A. (1972). *Mater. Res. Bull.* **7**, 1331–1338.
Sudarsanan, K. & Young, R. A. (1972). *Acta Cryst.* B**28**, 3668–3670.
Wardojo, T. A. & Hwu, S.-J. (1996). *Acta Cryst.* C**52**, 2959–2960.
White, T. J. & Dong, Z. L. (2003). *Acta Cryst.* B**59**, 1–16.
White, T. J., Segall, R. L. & Turner, P. S. (1985). *Angew. Chem. Int. Ed. Engl.* **24**, 357–365.
Wilhelmi, K. A. & Jonsson, O. (1965). *Acta Chem. Scand.* **19**, 177–184.
Wu, P., Zeng, Y. Z. & Wang, C. M. (2004). *Biomaterials*, **25**, 1123–1130.
Yasukawa, A., Kamiuchi, K., Yokoyama, T. & Ishikawa, T. (2002). *J. Solid State Chem.* **163**, 27–32.